Journal of Sound and Vibration 329 (2010) 3101–3120

Contents lists available at ScienceDirect

Journal of Sound and Vibration

journal homepage: www.elsevier.com/locate/jsvi

A substructure approach tailored to the dynamic analysis of multi-span continuous beams under moving loads

Vera De Salvo [a], Giuseppe Muscolino [a], Alessandro Palmeri [b,*]

[a] University of Messina, Department of Civil Engineering, Vill. S. Agata, 98166 Messina, Italy
[b] Loughborough University, Department of Civil and Building Engineering, Sir Frank Gibb Building, Loughborough LE11 3TU, UK

ARTICLE INFO

Article history:
Received 12 August 2009
Received in revised form
9 February 2010
Accepted 9 February 2010
Handling Editor: D.J. Thompson
Available online 11 March 2010

ABSTRACT

The paper deals with the dynamic analysis of multiply supported continuous beams subjected to moving loads, which in turn can be modelled either as moving forces or moving masses. A dedicated variant of the component mode synthesis (CMS) method is proposed in which the classical primary–secondary substructure approach (SA) is tailored to cope with slender (i.e. Euler–Bernoulli) continuous beams with arbitrary geometry. To do this, the whole structure is ideally decomposed in primary and secondary spans with convenient restraints, whose exact eigenfunctions are used as assumed local modes; the representation of the internal forces is improved with the help of two additional assumed modes for each primary span, while primary–secondary influence functions allow satisfying the kinematical compatibility between adjacent spans; the continuous beam is then re-assembled, and the Lagrange's equations of motion are derived in a compact block-matrix setting for both moving force and moving mass model. Numerical examples demonstrate accuracy and efficiency of the proposed procedure. An application with a platoon of high-speed moving masses confirms that the inertial effects neglected in the moving force model may have a significant impact in the structural response.

1. Introduction

In the general framework of vehicle-induced vibration of highway and railway bridges, the dynamics of multiply supported continuous beams under moving loads has been extensively studied, and several approaches are available in the literature, which differ in complexity and accuracy. In recent years, Lee proposed an approximate method for studying the transverse vibration of a multi-span Euler–Bernoulli beam subjected to moving forces [1] and moving masses [2], in which the assumed modes are the sinusoidal eigenfunctions of a homogenous simply supported beam, and the intermediate supports are modelled as linear springs with arbitrarily large rigidity. Since the assumed modes suggested in these papers do not satisfy the zero-deflection condition at the intermediate supports, Zheng et al. [3] proposed a modification consisting of cubic splines, in so eliminating the kinematical inconsistency. In the study by Ichikawa et al. [4], the exact eigenfunctions of homogeneous continuous beams have been derived and used to solve the moving mass problem; unfortunately, quite often this exact solution is of little help when real-life bridge engineering applications are dealt with, since the cross-sectional depth in actual continuous bridges increases in proximity of the intermediate supports. In order to overcome this drawback, Dugush and Eisenberger [5] derived the exact eigenfunctions of continuous beams with a

* Corresponding author. Tel.: +44 0 1509 222613; fax: +44 0 1509 223981.
E-mail addresses: a.palmeri@lboro.ac.uk, dynamics.structures@gmail.com (A. Palmeri).

0022-460X/$ - see front matter © 2010 Elsevier Ltd. All rights reserved.
doi:10.1016/j.jsv.2010.02.016

polynomial variation of the cross-sectional depth; in their formulation, however, only the moving force problem is addressed, and the structural damping is not taken into account, while the computation of the eigenfunctions may be cumbersome. Martínez-Castro et al. [6] pursed the solution of the moving force problem by discretizing the continuous beam with two-node Euler–Bernoulli elements of variable cross section, in conjunction with a semi-analytical scheme of dynamic analysis in the reduced modal space. Even thought of easy numerical implementation, this approach may require a large number of degrees of freedom, and the extension to the moving mass problem is not straightforward. Other investigations have been also focused on more specific aspects of continuous beams under moving loads, namely separation and re-attachment of vehicles [7], coupling conditions between adjacent spans [8] and identification problems [9]. Indeed, the persistent interest of researchers and engineers in this topic is justified both by the challenging nature of the governing equations [10] and also by the practical need of analysing the vibrations induced by high-speed trains crossing light bridge structures (e.g. Refs. [11–13]).

In this paper, aimed at overcoming the limitations of the methods available in the literature, a novel technique for the dynamic analysis of multi-span continuous beams traversed by moving forces and masses is proposed and numerically validated. The basic idea is to take advantage of the component mode synthesis (CMS) method (e.g. Refs. [14–18]), i.e. a substructure approach (SA) which proved to be particularly effective in treating continuous structures coupled with moving systems [19]. To do this, in a first stage the continuous beam is ideally decomposed into a series of alternate primary and secondary spans, whose BCs (boundary conditions) are conveniently selected; in a second stage, the Lagrange's equations of motion of the re-assembled continuous beam are derived, in which the kinematical compatibility is automatically satisfied at the interface between adjacent spans. In comparison with other CMS variants, the proposed approach lends itself to be easily automated, since the approximate modal shapes of the continuous beam are deduced from the eigenfunctions of pinned–pinned, pinned–clamped and clamped–clamped homogeneous beams, which are known in closed form [20]. The proposed SA has the additional advantage that the pertinent time-dependent matrices of mass, stiffness and damping are simply obtained by collocating the corresponding elementary blocks for each span within the global matrices; in turn, elementary blocks for primary and secondary subsystems are given in analytical form, which further reduces the computational burden.

For the sake of generality, the formulation is presented for the case of a stream of multiple forces and masses accelerating along the continuous beam, and the structural damping is also accounted for. Accuracy is demonstrated with two numerical applications taken from the literature, whose results are compared to those of previously published studies and conventional FEM (finite element method) analyses. A third numerical application with a platoon of high-speed moving masses is used to highlight the practical importance of the inertial effects neglected by the moving force model. Indeed, to the best of authors' knowledge, commercial FEM codes currently available for structural engineering purposes do not allow running dynamic analyses of bridges under a stream of moving masses.

2. Substructure approach (SA)

Let us consider the N-span Euler–Bernoulli continuous beam shown in Fig. 1a, where L and z are total length and global abscissa along the structure. Aimed at enabling analyses of actual bridges and vehicles, in this study the continuous beam is inhomogeneous (i.e. the cross section is allowed to vary with z), the positions of the intermediate supports are arbitrary, and the n_F moving forces travelling on the beam may have different intensity f_i, velocity $\dot{\xi}_i(t)$ and acceleration $\ddot{\xi}_i(t)$, $\xi_i(t)$ being the position of the generic i-th force ($i=1,\ldots,n_F$) at the time instant t.

The dynamic problem under consideration is ruled by the partial differential equation:

$$\mu(z)\frac{\partial^2}{\partial t^2}u(z,t)+D(z,t)+\frac{\partial^2}{\partial z^2}\left(\kappa(z)\frac{\partial^2}{\partial z^2}u(z,t)\right)=\sum_{i=1}^{n_F}f_i\delta(z-\xi_i(t)), \tag{1}$$

with the following boundary conditions (BCs):

$$u(0,t)=0;\quad \frac{\mathrm{d}^2}{\mathrm{d}z^2}u(z,t)|_{z=0}=0$$

$$u(L,t)=0;\quad \frac{\mathrm{d}^2}{\mathrm{d}z^2}u(z,t)|_{z=L}=0;$$

$$u\left(\bar{z}_i,t\right)=0,\quad i=2,\ldots,N-1. \tag{2a–e}$$

The functions $\mu(z)$ and $\kappa(z)$ in Eq. (1) are mass for unit length and flexural stiffness along the continuous beam, respectively; $u(z,t)$ is the time-dependent field of transverse displacements; $D(z,t)$ is the internal damping force per unit length. Moreover, the Dirac's delta function $\delta(z)$ in the right-hand side of Eq. (1) is defined as the formal derivative of the

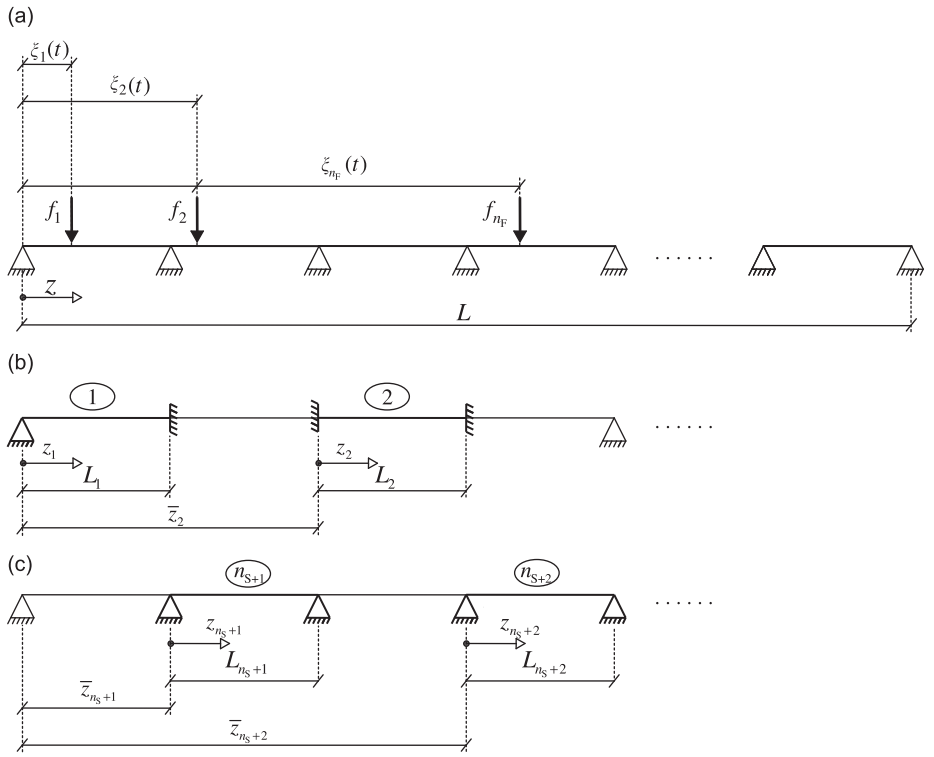

Fig. 1. Continuous beam under moving forces (a); secondary substructures with clamped ends at the position of the intermediate supports (b); primary substructures with pinned ends (c).

Heaviside's unit step function $U(z)$:

$$\delta(z)=\frac{\mathrm{d}}{\mathrm{d}z}\mathrm{U}(z);\quad \mathrm{U}(z)=\begin{cases}0 & z<0\\ \frac{1}{2} & z=0\\ 1 & z>0\end{cases} \tag{3a,b}$$

while $\overline{z}_i$ in Eq. (2) is the abscissa of the i-th internal support (Figs. 1b and c). It is worth mentioning that when spans become relatively short with respect to the depth of the continuous beam, the Euler–Bernoulli formulation may be inappropriate, and one may need to switch to the Timoshenko's theory of beams. This case is beyond the scope of the present paper.

2.1. Decomposition into primary and secondary spans

An exact solution for the dynamic problem in hand can be obtained in just a few situations, e.g. when inertia and rigidity do not vary along the structure (i.e. $\mu(z)$ and $\kappa(z)$ are constants), spans of the bridge have the same length (i.e. $L_i=L/N$, for $i=1,\ldots,N$) and all the moving loads do not accelerate/decelerate (i.e. $\ddot{\xi}_i(z)=0$, for $i=1,\ldots,n_F$). It follows that in most of actual design situations an exact solution is not available, and hence structural engineers must rely on approximate methods of analysis. Within this framework, the proposed formulation builds on the component mode synthesis (CMS) method, which lends itself to deal with moving load problems (e.g. Ref. [19]). Specifically, in order to particularize the classical primary–secondary substructure approach (SA), let the continuous beam be conveniently thought as composed of $n_S=\mathrm{int}[(N+1)/2]$ secondary spans (Fig. 1b) and $n_P=N-n_S$ primary spans (Fig. 1c). As illustrated in these sketches, substructures are numbered in such a way that indexes $i=1,\ldots,n_S$ denote secondary spans, while indexes $i=n_S+1,\ldots,n_S+n_P=N$ denote primary spans. It is also shown that, according to our decomposition, secondary and primary components alternate along the continuous beam. More precisely, the spans in odd position (first, third, and *etcetera*, from the left) are secondary substructures (Fig. 1b), while those in even position (second, fourth, and *etcetera*, from the left) are primary substructures (Fig. 1c).

The BCs of the substructures are imposed as follows: (i) the ends of the continuous beam are pinned, since this is the usual configuration in practice; (ii) the internal nodes at the position of the intermediate supports are assumed to be clamped for the secondary spans (Fig. 1b) and pinned for the primary ones (Fig. 1c), that is a free-fixed primary–secondary interface.

Once the whole structure has been decomposed in N elementary spans, the time-dependent field of displacement, $u(z,t)$, can be represented as

$$u(z,t)=\sum_{i=1}^{N} u_i(z-\overline{z}_i,t)\chi_i(z-\overline{z}_i), \tag{4}$$

where $u_i(z_i,t)$ is the deflection of the i-th span at local abscissa $z_i=z-\overline{z}_i$ and time instant t, while $\chi_i(z_i)$ is the window function for the i-th span (e.g. Ref. [21]):

$$\chi_i(z_i)=\mathrm{U}(z_i)-\mathrm{U}(z_i-L_i)=\begin{cases}1, & 0<z_i<L_i;\\ \dfrac{1}{2}, & z_i=0\ \ z_i=L_i;\\ 0, & z_i<0\ \ z_i>L.\end{cases} \tag{5}$$

It is worth mentioning that, given the numbering scheme of primary and secondary spans, the i-th abscissa $\overline{z}_i$ in Eq. (4) can be evaluated as

$$\overline{z}_i=\begin{cases}0, & i=1;\\ \displaystyle\sum_{k=1}^{i-1}(L_k+L_{n_S+k}), & 2\le i\le n_S;\\ \overline{z}_{i-n_S}+L_{i-n_S}, & n_S+1\le i\le N,\end{cases} \tag{6}$$

L_k being the length of the k-th span (see Fig. 1).

2.2. Assumed local modes for primary spans

Once the whole continuous beam has been decomposed into N individual spans, the transverse displacements for the generic i-th primary span ($i=n_S+1,\ldots,N$) can be expressed in the form:

$$u_i(z_i,t)=\sum_{j=1}^{m_i-2}\phi_{i,j}(z_i)q_{i,j}(t)+\phi_{i,m_i-1}(z_i)q_{i,m_i-1}(t)+\phi_{i,m_i}(z_i)q_{i,m_i}(t)=\boldsymbol{\phi}_i^T(z_i)\cdot\mathbf{q}_i(t), \tag{7}$$

where $\boldsymbol{\phi}_i(z_i)=\{\phi_{i,1}(z_i)\ \ \ldots\ \ \phi_{i,m_i-2}(z_i)|\phi_{i,m_i-1}(z_i)\ \ \phi_{i,m_i}(z_i)\}^{\mathrm{T}}$ is the array listing the m_i shape functions assumed for the i-th primary span, while $\mathbf{q}_i(t)=\{q_{i,1}(t)\ \ \ldots\ \ q_{i,m_i-2}(t)|q_{i,m_i-1}(t)\ \ q_{i,m_i}(t)\}^{\mathrm{T}}$ is the array of the corresponding generalized displacements. The array $\boldsymbol{\phi}_i(z_i)$ has been partitioned in order to highlight the last two assumed modes, which are defined differently with respect to the first ones. More precisely, among all the possible choices, we take as first (m_i-2) assumed modes the eigenfunctions of the homogenized beam having averaged values of mass for unit length, $\overline{\mu}_i$, and flexural stiffness, $\overline{\kappa}_i$:

$$\overline{\mu}_i=\frac{\rho}{L_i}\int_0^{L_i}A_i(z_i)\,\mathrm{d}z_i;\quad \overline{\kappa}_i=\frac{E}{L_i}\int_0^{L_i}J_i(z_i)\,\mathrm{d}z_i, \tag{8a,b}$$

where ρ and E are mass density and Young's modulus of the material, respectively, while $A_i(z_i)$ describes the variation of the cross-sectional area along the i-th span, and $J_i(z_i)$ the corresponding second moment.

The shape functions $\phi_{i,j}(z_i)$, then, are obtained as solution of the classical eigenproblem ($j=1,2,\ldots,m_i-2$):

$$\overline{\kappa}_i\frac{\mathrm{d}^4}{\mathrm{d}z_i^4}\phi_{i,j}(z_i)=\omega_{i,j}^2\overline{\mu}_i\phi_{i,j}(z_i), \tag{9}$$

with pinned–pinned BCs (see Fig. 1c):

$$\phi_{i,j}(0)=0;\quad \phi_{i,j}(L_i)=0;\quad \left.\frac{\mathrm{d}^2\phi_{i,j}(z_i)}{\mathrm{d}z_i^2}\right|_{z_i=0}=0;\quad \left.\frac{\mathrm{d}^2\phi_{i,j}(z_i)}{\mathrm{d}z_i^2}\right|_{z_i=L_i}=0, \tag{10a–d}$$

and subjected to the ortho-normalization condition:

$$\overline{\mu}_i\int_0^{L_i}\phi_{i,j}(z_i)\phi_{i,k}(z_i)\mathrm{d}z_i=\delta_{j,k}, \tag{11}$$

$\delta_{j,k}$ being the Kronecker's delta symbol, equal to one when $j=k$, zero otherwise. Thus, the first assumed modes for the primary spans turn out to be sinusoidal functions given by ($i=n_S+1,\ldots,N$; $j=1,2,\ldots,m_i-2$)

$$\phi_{i,j}(z_i)=\sqrt{\frac{2}{\overline{\mu}_iL_i}}\sin\left(\frac{j\pi z_i}{L_i}\right). \tag{12}$$

For illustrative purposes, the first assumed mode of the first primary beam, namely the function $\phi_{n_S+1,1}(z_{n_S+1})$, is shown in Fig. 2c.

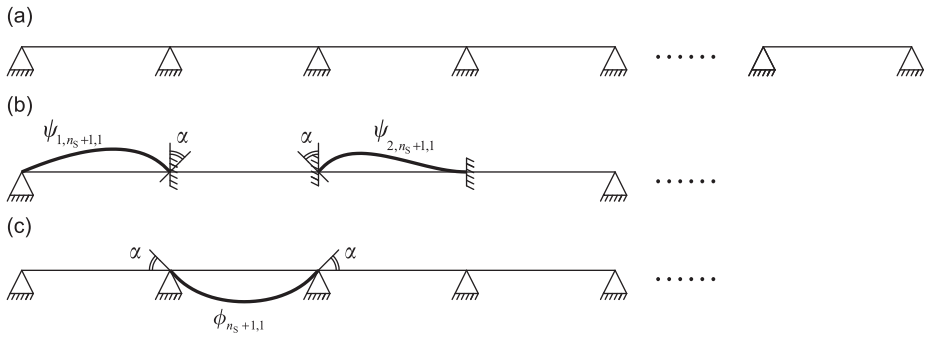

Fig. 2. Reference sketch of the continuous beam (a); first eigenfunction selected as assumed local mode for the first primary span (c); influence functions on the adjacent secondary spans, which re-establish the compatibility between primary and secondary substructures (b).

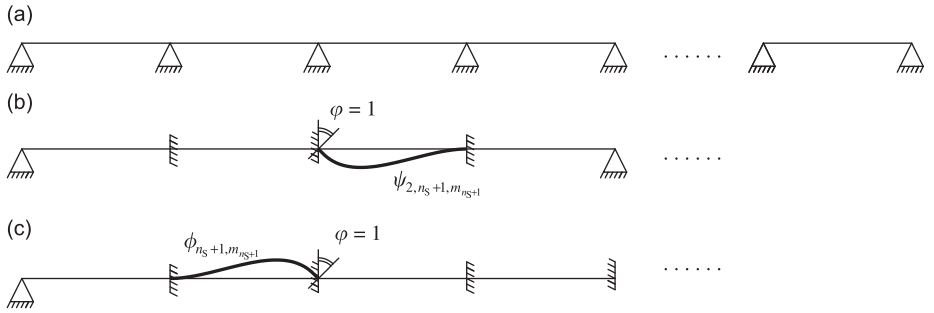

Fig. 3. Reference sketch of the continuous beam (a); last assumed local mode for the first primary span (c); influence functions on the adjacent secondary span (b).

Although for engineering purposes these sinusoidal functions are able to describe accurately the transverse deflection along the i-th primary span, the bending moment (BM) diagram cannot be represented adequately without enlarging properly the set of assumed modes. Indeed, consistently to the pinned–pinned BCs, the value of the BM associated with the eigenfunctions of Eq. (12) is zero at the ends of the i-th primary span (i.e. both at $z_i=0$ and at $z_i=L_i$), while in practice a peak of the BM diagram is expected at the position of the intermediate supports in the actual continuous beam.

To overcome this flaw, the last two assumed modes in the array $\boldsymbol{\phi}_i(z_i)$ for primary spans are chosen as the deformed shapes of the homogenized spans with clamped–clamped BCs and subjected to a unit rotation alternatively at each of the two ends. For the i-th primary span these two additional functions are solution of the following fourth-order differential equation ($j=m_i-1$, m_i):

$$\frac{\mathrm{d}^4}{\mathrm{d}z_i^4}\phi_{i,j}(z_i)=0, \tag{13}$$

with BCs:

$$\phi_{i,j}(0)=0; \quad \phi_{i,j}(L_i)=0; \quad \left.\frac{\mathrm{d}\phi_{i,j}(z_i)}{\mathrm{d}z_i}\right|_{z_i=0}=\delta_{m_i-1,j}; \quad \left.\frac{\mathrm{d}\phi_{i,j}(z_i)}{\mathrm{d}z_i}\right|_{z_i=L_i}=\delta_{m_i,j}, \tag{14a–d}$$

and subjected to the normalization condition:

$$\overline{\mu}_i\int_0^{L_i}[\phi_{i,j}(z_i)]^2\mathrm{d}z_i=1. \tag{15}$$

One can easily prove that the new complementary assumed modes take the cubic expressions:

$$\phi_{i,m_i-1}(z_i)=\sqrt{\frac{105}{\overline{\mu}_i L_i}}\left(1-\frac{z_i}{L_i}\right)^2\frac{z_i}{L_i}; \quad \phi_{i,m_i}(z_i)=\sqrt{\frac{105}{\overline{\mu}_i L_i}}\left(1-\frac{z_i}{L_i}\right)\left(\frac{z_i}{L_i}\right)^2. \tag{16a,b}$$

The second of these functions is qualitatively shown in Fig. 3c, where the righ-hand side end of the first primary beam ($i=n_S+1$) is subjected to an unitary clockwise rotation ($\varphi=1$ in the sketch).

2.3. Assumed local modes for secondary spans

According to the component mode synthesis (CMS) method (e.g. Refs. [14–18]), the field of displacement for the generic secondary substructure is expressed as the superposition of two contributions. In the problem in hand, the first contribution describes the transverse displacements of the i-th secondary span assumed to be clamped at the internal supports, while the second contribution satisfies the compatibility conditions with adjacent primary spans:

$$u_i(z_i,t)=\sum_{j=1}^{m_i}\phi_{i,j}(z_i)q_{i,j}(t)+\sum_{k=n_S+1}^{N}\sum_{j=1}^{m_k}\psi_{i,k,j}(z_i)q_{k,j}(t)=\boldsymbol{\phi}_i^T(z_i)\cdot\mathbf{q}_i(t)+\sum_{k=n_S+1}^{N}\boldsymbol{\psi}_{i,k}^T(z_i)\cdot\mathbf{q}_k(t), \tag{17}$$

where, the m_i-dimensional arrays $\boldsymbol{\phi}_i(z_i)=\{\phi_{i,1}(z_i)\ \ \dots\ \ \phi_{i,m_i}(z_i)\}^{\mathrm{T}}$ and $\mathbf{q}_i(t)=\{q_{i,1}(t)\ \ \dots\ \ q_{i,m_i}(t)\}^{\mathrm{T}}$ list shape functions and generalized displacements for the i-th span, respectively, while $\boldsymbol{\psi}_{i,k}(z_i)=\{\psi_{i,k,1}(z_i)\ \ \dots\ \ \psi_{i,k,m_k}(z_i)\}^{\mathrm{T}}$ is the array collecting the m_k influence functions of the primary spans.

Similarly to the previous subsection, the assumed modes $\phi_{i,j}(z_i)$ are the eigenfunctions of the homogenized span (see Eqs. (8)), which are solution of the same eigenproblem of Eq. (9), but with different BCs (see Fig. 1b). Specifically, for an inner secondary span, the BCs read:

$$\phi_{i,j}(0)=0;\quad \phi_{i,j}(L_i)=0;\quad \left.\frac{\mathrm{d}\phi_{i,j}(z_i)}{\mathrm{d}z_i}\right|_{z_i=0}=\left.\frac{\mathrm{d}\phi_{i,j}(z_i)}{\mathrm{d}z_i}\right|_{z_i=L_i}=0, \tag{18a–d}$$

and the solution can be posed in the form [20]:

$$\begin{aligned}\phi_{i,j}(z_i)=\frac{a_{i,j}}{\sinh(\beta_{i,j}L_i)-\sin(\beta_{i,j}L_i)}\times\Big\{&\cosh(\beta_{i,j}z_i)\sinh(\beta_{i,j}L_i)-\cosh(\beta_{i,j}L_i)\sinh(\beta_{i,j}z_i)\\&-\cos(\beta_{i,j}z_i)\sinh(\beta_{i,j}L_i)+\cos(\beta_{i,j}L_i)\sinh(\beta_{i,j}z_i)-\cosh(\beta_{i,j}z_i)sin(\beta_{i,j}L_i)\\&+\cosh(\beta_{i,j}L_i)\sin(\beta_{i,j}z_i)+\cos(\beta_{i,j}z_i)\sin(\beta_{i,j}L_i)+\cos(\beta_{i,j}L_i)\sin(\beta_{i,j}z_i)\Big\},\end{aligned} \tag{19}$$

where the coefficient $\beta_{i,j}$ is the j-th non-trivial root of the characteristic equation:

$$\cos(\beta_{i,j}L_i)=\frac{1}{\cosh(\beta_{i,j}L_i)}, \tag{20}$$

while the value of the normalization coefficient $a_{i,j}$ is computed in order to satisfy the condition:

$$\overline{\mu}_i\int_0^{L_i}[\phi_{i,j}(z_i)]^2\mathrm{d}z_i=1. \tag{21}$$

It is worth noting that, although more complicated than the analytical expressions reported in many textbooks of structural dynamics, Eq. (19) virtually eliminates the round-off errors in the floating-point math imposed by digital computers [20], which make the classical expressions not suitable for numerical computations. For the sake of completeness, the first twelve roots of Eq. (20) are listed in Table 1 (top).

As shown in Fig. 1b, the BCs for the left-hand side span (i=1) are pinned–clamped:

$$\phi_{1,j}(0)=0;\quad \phi_{1,j}(L_1)=0;\quad \left.\frac{\mathrm{d}^2\phi_{1,j}(z_1)}{\mathrm{d}z_1^2}\right|_{z_1=0}=0;\quad \left.\frac{\mathrm{d}\phi_{1,j}(z_1)}{\mathrm{d}z_1}\right|_{z_1=L_1}=0. \tag{22a–d}$$

Table 1
First non-trivial roots of the characteristic equations for homogeneous clamped–clamped (Eq. (20)) and pinned-clamped (Eq. (24)) beams.

j	$\beta_{i,j}L_i$	j	$\beta_{i,j}L_i$	j	$\beta_{i,j}L_i$
Clamped–clamped					
1	4.730041	5	17.278760	9	29.845130
2	7.853205	6	20.420352	10	32.986723
3	10.995608	7	23.561945	11	36.128316
4	14.137165	8	26.703538	12	39.269908
Pinned–clamped					
1	1.875104	5	14.137168	9	26.703538
2	4.694091	6	17.278760	10	29.845130
3	7.854757	7	20.420352	11	32.986723
4	10.995541	8	23.561945	12	36.128316

Therefore, the solution of Eq. (9) for this span can be posed in the form [20]:

$$\phi_{1,j}(z_i) = \frac{a_{1,j}}{\sinh(\beta_{1,j}L_1)+\sin(\beta_{1,j}L_1)} \times \cosh(\beta_{1,j}L_1-\beta_{1,j}z_1)\sinh(\beta_{1,j}L_1)-\cosh(\beta_{1,j}L_1)\sinh(\beta_{1,j}L_1-\beta_{1,j}z_1)$$
$$-\cos(\beta_{1,j}L_1-\beta_{1,j}z_1)\sinh(\beta_{1,j}L_1)-\cos(\beta_{1,j}L_1)\sinh(\beta_{1,j}L_1-\beta_{1,j}z_1)+\cos h(\beta_{1,j}L_1-\beta_{1,j}z_1)\sin(\beta_{1,j}L_1)$$
$$+\cosh(\beta_{1,j}L_1)\sin(\beta_{1,j}L_1-\beta_{1,j}z_1)-\cos(\beta_{1,j}L_1-\beta_{1,j}z_1)\sin(\beta_{1,j}L_1)+\cos(\beta_{1,j}L_1)\sin(\beta_{1,j}L_1-\beta_{1,j}z_1)\}, \quad (23)$$

in which $\beta_{1,j}$ is the j-th root of the characteristic equation:

$$\cos(\beta_{1,j}L_1) = -\frac{1}{\cosh(\beta_{1,j}L_1)}, \quad (24)$$

and again $a_{1,j}$ is the normalization constant satisfying the condition:

$$\overline{\mu}_1 \int_0^{L_i} [\phi_{1,j}(z_1)]^2 dz_1 = 1. \quad (25)$$

The first twelve roots of Eq. (24) are listed in Table 1 (bottom).

When the total number of spans N is odd, the last secondary span has mirrored BCs with respect to the first one, i.e. clamped–pinned instead of pinned–clamped. In this case the assumed modes $\phi_{n_S,j}(z_{n_S})$ can be directly derived from Eqs. (23)–(25), valid for the first secondary span, and are not reported here.

For illustrative purposes, the first assumed modes for lateral and internal primary beams, namely the functions $\phi_{1,1}(z_1)$ and $\phi_{2,1}(z_2)$, are shown in Fig. 4b.

2.4. Influence functions of primary spans on secondary spans

In order to complete the representation of the transverse displacements experienced by secondary spans, the influence functions $\psi_{i,k,j}(z_i)$ appearing in Eq. (17) must be defined. Since the purpose of these additional assumed modes is to re-establish the compatibility among adjacent spans, $\psi_{i,k,j}(z_i)$ is in our model the static deformed shapes of the i-th secondary span ($i=1,\ldots,n_S$) obtained by imposing the compatibility in terms of rotation with the j-th assumed mode ($j=1,\ldots,m_k$) of the k-th primary span ($k=n_S+1,\ldots,N$). Accordingly, when i-th and k-th spans are not adjacent, $\psi_{i,k,j}(z_i) \equiv 0$. Otherwise, $\psi_{i,k,j}(z_i)$ can be sought as solution of the following fourth-order differential equation:

$$\frac{d^2}{dz_i^2}\left(J_i(z_i)\frac{d^2}{dz_i^2}\psi_{i,k,j}(z_i)\right) = 0. \quad (26)$$

For $i=k-n_S$, i-th secondary span precedes k-th primary span (e.g. $i=1$ and $k=n_S+1$), and the compatibility must be enforced at the right-hand side of the secondary span:

$$\psi_{i,k,j}(L_i) = 0; \quad \left.\frac{d\psi_{i,k,j}(z_i)}{dz_i}\right|_{z_i=L_i} = \left.\frac{d\phi_{k,j}(z_k)}{dz_k}\right|_{z_k=0}. \quad (27a,b)$$

On the contrary, for $i=k-n_S+1$, i-th secondary span succeeds k-th primary span (e.g. $i=2$ and $k=n_S+1$), and hence the compatibility must be re-established at the left-hand side of the secondary span:

$$\psi_{i,k,j}(0) = 0; \quad \left.\frac{d\psi_{i,k,j}(z_i)}{dz_i}\right|_{z_i=0} = \left.\frac{d\phi_{k,j}(z_k)}{dz_k}\right|_{z_k=L_k}. \quad (28a,b)$$

If the $J_i(z_i)$ is either constant (homogeneous span) or a polynomial function of the local abscissa z_i, Eq. (26) can be solved in closed form; otherwise, a numerical method of solution can be used.

In order to visualize the compatibility conditions between primary and secondary spans, the pertinent primary–secondary influence functions are sketched in Figs. 2b and 3b.

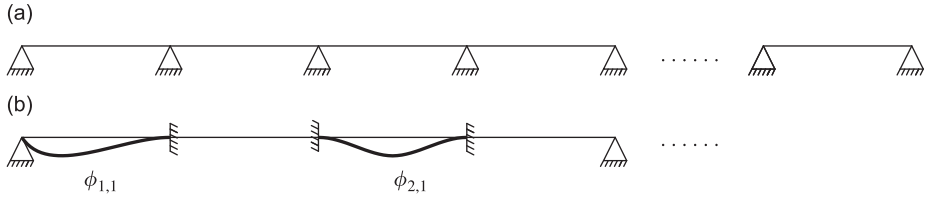

Fig. 4. Reference sketch of the continuous beam (a); first eigenfunctions selected as assumed local modes for first (lateral) and third (internal) secondary spans (b).

3. Lagrange's equations of motion: moving force problem

In the previous section, the assumed modes for each span of the continuous beam have been presented. These local trial functions approximate the actual field of transverse displacements throughout the structure, and automatically satisfy the global BCs for the whole continuous beam along with the kinematical compatibility between adjacent spans. In order to derive the equations of motion for the entire structure, let us consider the Lagrangian function $\overline{\mathcal{L}}$ (e.g. Refs. [22–24]) for the dynamic system in hand:

$$\overline{\mathcal{L}} = \overline{T} - \overline{V}, \tag{29}$$

where the explicit dependence on time t has been omitted in order to simplify the notation. By exploiting Eq. (4), kinetic energy $\overline{T}$ and potential energy $\overline{V}$ in the right-hand side of Eq. (29) can be expressed as the sum of N contributions, one for each span:

$$\overline{T} = \frac{1}{2}\int_0^L \mu(z)\left[\frac{\partial}{\partial t}u(z,t)\right]^2 \mathrm{d}z = \frac{1}{2}\rho\sum_{i=1}^{N}\int_0^{L_i} A_i(z_i)\left[\frac{\partial}{\partial t}u_i(z_i,t)\right]^2 \mathrm{d}z_i; \tag{30}$$

$$\overline{V} = \frac{1}{2}\left\{\int_0^{L_i}\kappa(z)\left[\frac{\partial^2}{\partial z^2}u(z,t)\right]^2 \mathrm{d}z - g\int_0^{L_i}\mu(z)u(z,t)\,\mathrm{d}z\right\} = \frac{1}{2}\sum_{i=1}^{N}\left\{E\int_0^{L_i} J_i(z_i)\left[\frac{\partial^2}{\partial z_i^2}u_i(z_i,t)\right]^2 \mathrm{d}z_i - g\rho\int_0^{L_i} A_i(z_i)u_i(z_i,t)\,\mathrm{d}z_i\right\}, \tag{31}$$

where g is the acceleration of gravity, while the functions $\mu(z)$ and $\kappa(z)$ have been represented similarly to Eq. (4):

$$\mu(z) = \rho\sum_{i=1}^{N} A_i(z-\overline{z}_i)\chi_i(z-\overline{z}_i); \quad \kappa(z) = E\sum_{i=1}^{N} J_i(z-\overline{z}_i)\chi_i(z-\overline{z}_i). \tag{32a,b}$$

According to Eqs. (7) and (17), the deformed shape of the continuous beam at a given time instant t depends on the generalized coordinates listed in the N arrays $\mathbf{q}_i(t)$, with $i=1, \ldots, N$. Therefore, the Lagrange's equations of motion for the i-th span take the form:

$$\frac{\mathrm{d}}{\mathrm{d}t}\left[\frac{\partial}{\partial\dot{\mathbf{q}}_i}\overline{\mathcal{L}}\right] - \frac{\partial}{\partial\mathbf{q}_i}\overline{\mathcal{L}} + \frac{\partial}{\partial\dot{\mathbf{q}}_i}\mathcal{R} = \overline{\mathbf{Q}}_i(t), \quad i = 1,2,\ldots,N, \tag{33}$$

in which $\mathcal{R}$ is the so-called Rayleigh's dissipation function (e.g. Refs. [22,24]), i.e. a quadratic form of the arrays $\dot{\mathbf{q}}_i(t)$, and $\overline{\mathbf{Q}}_i(t)$ is the generalized excitation associated with the i-th arrays $\mathbf{q}_i(t)$ for the moving force problem:

$$\overline{\mathbf{Q}}_i(t) = \sum_{k=1}^{n_F} f_k\frac{\partial}{\partial\mathbf{q}_i}u(\xi_k(t),t) = \sum_{k=1}^{n_F}\sum_{i=1}^{N} f_k\chi_i(\xi_k(t)-\overline{z}_i)\frac{\partial}{\partial\mathbf{q}_i}u_i(\xi_k(t)-\overline{z}_i,t). \tag{34}$$

Upon substitution of Eqs. (7) and (17) into Eqs. (33) and (34), the equations of motion for the secondary spans can be written as ($i=1, \ldots, n_S$):

$$\overline{\mathbf{m}}_{i,i}^{(\mathrm{SS})}\cdot\ddot{\mathbf{q}}_i(t) + \sum_{j=n_S+1}^{N}\overline{\mathbf{m}}_{i,j}^{(\mathrm{SP})}\cdot\ddot{\mathbf{q}}_j(t) + \sum_{j=1}^{n_S}\overline{\mathbf{c}}_{i,j}^{(\mathrm{SS})}\cdot\dot{\mathbf{q}}_j(t) + \sum_{j=n_S+1}^{N}\overline{\mathbf{c}}_{i,j}^{(\mathrm{SP})}\cdot\dot{\mathbf{q}}_j(t) + \overline{\mathbf{k}}_{i,i}^{(\mathrm{SS})}\cdot\mathbf{q}_i(t) = \overline{\mathbf{f}}_i^{(\mathrm{S})}(t), \tag{35}$$

while for the n_P primary spans ($i=n_S+1, \ldots, N$):

$$\sum_{j=n_S+1}^{N}\overline{\mathbf{m}}_{i,j}^{(\mathrm{PP})}\cdot\ddot{\mathbf{q}}_j(t) + \sum_{j=1}^{n_S}\overline{\mathbf{m}}_{i,j}^{(\mathrm{PS})}\cdot\ddot{\mathbf{q}}_j(t) + \sum_{j=n_S+1}^{N}\overline{\mathbf{c}}_{i,j}^{(\mathrm{PP})}\cdot\dot{\mathbf{q}}_j(t) + \sum_{j=1}^{n_S}\overline{\mathbf{c}}_{i,j}^{(\mathrm{PS})}\cdot\dot{\mathbf{q}}_j(t) + \sum_{j=n_S+1}^{N}\overline{\mathbf{k}}_{i,j}^{(\mathrm{PP})}\cdot\mathbf{q}_j(t) = \overline{\mathbf{f}}_i^{(\mathrm{P})}(t). \tag{36}$$

In Eqs. (35) and (36), the symbols $\overline{\mathbf{m}}$, $\overline{\mathbf{c}}$ and $\overline{\mathbf{k}}$ denote mass, damping and stiffness matrices, respectively; the symbols $\overline{\mathbf{f}}$ denote the loading vectors; the superscripts S and P stand for secondary and primary spans, respectively. Once the super-array $\mathbf{q}(t)$, listing all the $M = \sum_{i=1}^{N} m_i$ generalized coordinates of the N spans has been introduced:

$$\mathbf{q}(t) = \left\{\mathbf{q}_1^{\mathrm{T}}(t) \;\ldots\; \mathbf{q}_{n_S}^{\mathrm{T}}(t) | \mathbf{q}_{n_S+1}^{\mathrm{T}}(t) \;\ldots\; \mathbf{q}_N^{\mathrm{T}}(t)\right\}^{\mathrm{T}}, \tag{37}$$

Eqs. (35) and (36) can be arranged in the more compact form:

$$\overline{\mathbf{M}}\cdot\ddot{\mathbf{q}}(t) + \overline{\mathbf{C}}\cdot\dot{\mathbf{q}}(t) + \overline{\mathbf{K}}\cdot\mathbf{q}(t) = \overline{\mathbf{f}}(t). \tag{38}$$

M-dimensional matrix of inertia, $\overline{\mathbf{M}}$, stiffness matrix, $\overline{\mathbf{K}}$, and loading vector, $\overline{\mathbf{f}}(t)$, can be automatically assembled starting from the corresponding quantities appearing in Eqs. (35) and (36), whose definition is given is Appendix A:

$$\overline{\mathbf{M}} = \begin{bmatrix} \ddots & & \vdots & \iddots \\ & \overline{\mathbf{m}}_{i,i}^{(SS)} & \cdots \; \overline{\mathbf{m}}_{i,j}^{(SP)} & \cdots \\ & & \ddots & \vdots \\ & \text{sym} & \cdots \; \overline{\mathbf{m}}_{i,j}^{(PP)} & \cdots \\ & & \iddots & \ddots \end{bmatrix}; \tag{39a}$$

$$\overline{\mathbf{K}} = \begin{bmatrix} \ddots & & & \\ & \overline{\mathbf{k}}_{i,i}^{(SS)} & & \\ & & \ddots & \\ & & & \ddots \; \vdots \; \iddots \\ & & & \cdots \; \overline{\mathbf{k}}_{i,j}^{(PP)} \; \cdots \\ & & & \iddots \; \vdots \; \ddots \end{bmatrix}; \quad \overline{\mathbf{f}}(t) = \begin{bmatrix} \vdots \\ \overline{\mathbf{f}}_i^{(S)}(t) \\ \vdots \\ \overline{\mathbf{f}}_i^{(P)}(t) \\ \vdots \end{bmatrix}, \tag{39b,c}$$

while, in order to have the same viscous damping ratio ζ in all the modes of vibration, the damping matrix, $\overline{\mathbf{C}}$, can be defined as follows:

$$\overline{\mathbf{C}} = 2\zeta \overline{\mathbf{M}} \cdot \overline{\mathbf{A}} \cdot \overline{\mathbf{\Omega}} \cdot \overline{\mathbf{A}}^{\mathrm{T}} \cdot \overline{\mathbf{M}}, \tag{40}$$

where spectral matrix $\overline{\mathbf{\Omega}}$ and modal matrix $\overline{\mathbf{A}}$ are solution of the eigenproblem:

$$\overline{\mathbf{K}} \cdot \overline{\mathbf{A}} = \overline{\mathbf{M}} \cdot \overline{\mathbf{A}} \cdot \overline{\mathbf{\Omega}}^2, \tag{41}$$

with the normalization condition $\overline{\mathbf{A}}^{\mathrm{T}} \cdot \overline{\mathbf{M}} \cdot \overline{\mathbf{A}} = \mathbf{I}_M$, $\mathbf{I}_M$ being the identity matrix of size M.

It is worth noting that the particular choice of the shape functions $\phi_{i,j}(z_i)$ and $\psi_{i,k,j}(z_i)$ for the N spans implies that the stiffness matrix of the continuous beam, $\overline{\mathbf{K}}$, is block-diagonal (see. Eq. (39b)), i.e. there is no coupling in terms of stiffness coefficients between the generalized displacements associated with secondary and primary spans. Moreover, the (SS) upper-left blocks of both mass and stiffness matrices are block-diagonal itself (see. Eqs. (39a) and (39b)), i.e. there is no coupling in terms of inertial and stiffness coefficients between different secondary spans.

Once the matrices $\overline{\mathbf{M}}$, $\overline{\mathbf{C}}$ and $\overline{\mathbf{K}}$ have been assembled along with the loading array $\overline{\mathbf{f}}(t)$, the dynamic response of the continuous beam can be obtained: first, by solving numerically Eq. (38), e.g. with the unconditionally stable Newmark's β method [25] with parameters β=1/4 and γ=1/2 (constant average acceleration method); second, by projecting the time histories of generalized coordinates listed in the super-array $\mathbf{q}(t)$, onto the actual fields of time-dependent transverse displacements and internal forces.

Upon substitution of Eqs. (7) and (17) into Eq. (4), and conveniently rearranging the resulting expression, the time history of deflections experienced by the continuous beam can be represented in a unified form as

$$u(z,t) = \sum_{i=1}^{N} \chi_i(z-\overline{z}_i)\boldsymbol{\phi}_i^{\mathrm{T}}(z-\overline{z}_i) \cdot \mathbf{q}_i(t) + \sum_{i=1}^{n_S} \sum_{k=n_S+1}^{N} \chi_i(z-\overline{z}_i)\boldsymbol{\psi}_{i,k}^{T}(z-z_i) \cdot \mathbf{q}_k(t), \tag{42}$$

which is valid for both primary and secondary spans. Bending moment (BM) $\mathcal{M}(z,t)$ and shear force (SF) $\mathcal{V}(z,t)$ along the continuous beam can be evaluated according to the Euler–Bernoulli theory of slender beams in bending. After simple manipulations, the internal forces take expressions similar to Eq. (42):

$$\mathcal{M}(z,t) = -E\left(\sum_{i=1}^{N} \chi_i(z-\overline{z}_i)\{J_i(z-\overline{z}_i)\boldsymbol{\phi}_i''(z-\overline{z}_i)\}^{\mathrm{T}} \cdot \mathbf{q}_i(t) + \sum_{i=1}^{n_S} \sum_{k=n_S+1}^{N} \chi_i(z-\overline{z}_i)\{J_i(z-\overline{z}_i)\boldsymbol{\psi}_{i,k}''(z-z_i)\}^{\mathrm{T}} \cdot \mathbf{q}_k(t) \right); \tag{43a}$$

$$\begin{aligned} \mathcal{V}(z,t) = -E\Bigg(& \sum_{i=1}^{N} \chi_i(z-\overline{z}_i)\{J_i(z-\overline{z}_i)\boldsymbol{\phi}_i'''(z-\overline{z}_i) + J_i'(z-\overline{z}_i)\boldsymbol{\phi}_i''(z-\overline{z}_i)\}^{\mathrm{T}} \cdot \mathbf{q}_i(t) \\ & + \sum_{i=1}^{n_S} \sum_{k=n_S+1}^{N} \chi_i(z-\overline{z}_i)\{J_i(z-\overline{z}_i)\boldsymbol{\psi}_{i,k}'''(z-\overline{z}_i) + J_i'(z-\overline{z}_i)\boldsymbol{\psi}_{i,k}''(z-\overline{z}_i)\}^{\mathrm{T}} \cdot \mathbf{q}_k(t) \Bigg), \end{aligned} \tag{43b}$$

where the prime denotes derivation with respect to the abscissa z.

The accuracy in the evaluation of BM and SF can be further improved by using a proper modal correction method (e.g. Ref. [26]).

4. Lagrange's equations of motion: moving mass problem

In previous section, the equations of motion of a continuous beam carrying n_F moving forces have been derived. Although very popular for practical applications, the moving force model is the crudest approximation known to the literature for studying the vibration of a bridge traversed by vehicles. When the inertia of vehicles cannot be regarded as small with respect to the mass of the bridge, however, moving forces should be substituted by a set of corresponding moving masses (e.g. Refs. [27–29]). Unfortunately, this improved representation of moving loads complicates significantly the governing equations [10], and hence conventional FEM (finite element method) codes do not allow this type of analysis. Aim of this section is to derive the equations of motion of a continuous beam subjected to a platoon of n_M moving masses, in so showing the versatility of the proposed primary–secondary SA.

With respect to the previous case, total kinetic energy and total potential energy include now the additional contributions due to the n_M moving masses:

$$\tilde{T} = \overline{T} + \sum_{k=1}^{n_M} \Delta T_k; \quad \tilde{V} = \overline{V} + \sum_{k=1}^{n_M} \Delta V_k. \tag{44a,b}$$

The increment of the total kinetic energy due to the k-th mass is given by

$$\begin{aligned}\Delta T_k &= \frac{1}{2} M_k \left[\dot{\xi}_k^2(t) + \left(\frac{\partial}{\partial t} u(\xi_k(t), t) + \dot{\xi}_k(t) \frac{\partial}{\partial z} u(\xi_k(t), t) \right)^2 \right] \\ &= \frac{1}{2} M_k \left[\dot{\xi}_k^2(t) + \sum_{i=1}^{N} \left(\frac{\partial}{\partial t} u_i(\xi_k(t) - \overline{z}_i, t) + \dot{\xi}_k(t) \frac{\partial}{\partial z_i} u_i(\xi_k(t) - \overline{z}_i, t) \right)^2 \chi_i(\xi_k(t) - \overline{z}_i) \right],\end{aligned} \tag{45}$$

in which $M_k = f_k/g$ is the k-th moving mass, $\dot{\xi}_k(t)$ is the horizontal component of its velocity, while the vertical component is the sum of two terms, which are related to the partial derivatives of the beam's transverse displacements with respect to time t and abscissa z, respectively.

The increment of the total potential energy due to the k-th mass is given by

$$\Delta V_k = -g M_k u(\xi_k(t), t) = -g M_k \sum_{i=1}^{N} u_i(\xi_k(t) - \overline{z}_i, t) \chi_i(\xi_k(t) - \overline{z}_i). \tag{46}$$

Furthermore, since there are no external forces acting on the system (i.e. the moving masses must be regarded as part of the dynamic system rather than external excitations), the right-hand side of Eq. (33) vanishes:

$$\tilde{\mathbf{Q}}_i(t) = \mathbf{0}. \tag{47}$$

Taking into account Eqs. (44)–(47), the Lagrange's equations of motion for the moving mass problem lead to

$$\tilde{\mathbf{M}}(t) \cdot \ddot{\mathbf{q}}(t) + \tilde{\mathbf{C}}(t) \cdot \dot{\mathbf{q}}(t) + \tilde{\mathbf{K}}(t) \cdot \mathbf{q}(t) = \tilde{\mathbf{f}}(t), \tag{48}$$

in which mass, damping and stiffness matrices are those provided in the previous section for the moving forces, incremented by the time-dependent sparse matrices $\Delta\mathbf{M}(t)$, $\Delta\mathbf{C}(t)$ and $\Delta\mathbf{K}(t)$, respectively, which take into account the inertial effects due to the moving masses. That is, $\tilde{\mathbf{M}}(t) = \overline{\mathbf{M}} + \Delta\mathbf{M}(t)$, $\tilde{\mathbf{K}}(t) = \overline{\mathbf{K}} + \Delta\mathbf{K}(t)$ and $\tilde{\mathbf{C}}(t) = \overline{\mathbf{C}} + \Delta\mathbf{C}(t)$. Moreover, the loading vector, $\tilde{\mathbf{f}}(t)$ is different too. The new quantities can be assembled as

$$\Delta\mathbf{M}(t) = \begin{bmatrix} \ddots & & \vdots & \iddots \\ & \Delta\mathbf{m}_{i,i}^{(SS)}(t) & \cdots \; \Delta\mathbf{m}_{i,j}^{(SP)}(t) & \cdots \\ & & \vdots & \\ & \text{sym} & \cdots \; \Delta\mathbf{m}_{j,j}^{(PP)}(t) & \cdots \\ & & \vdots & \ddots \end{bmatrix}; \tag{49a}$$

$$\Delta\mathbf{C}(t) = \begin{bmatrix} \ddots & & \vdots & \iddots \\ & \Delta\mathbf{c}_{i,i}^{(SS)}(t) & \cdots \; \Delta\mathbf{c}_{i,j}^{(SP)}(t) & \cdots \\ & & \vdots & \\ \cdots & \Delta\mathbf{c}_{j,i}^{(PS)}(t) & \cdots \; \Delta\mathbf{c}_{j,j}^{(PP)}(t) & \cdots \\ \iddots & \vdots & \ddots & \end{bmatrix}; \tag{49b}$$

$$\Delta\mathbf{K}(t)=\begin{bmatrix} \ddots & & \vdots & \\ & \Delta\mathbf{k}_{i,i}^{(SS)}(t) & \cdots & \Delta\mathbf{k}_{i,j}^{(SP)}(t) & \cdots \\ & \vdots & & \vdots & \\ \cdots & \Delta\mathbf{k}_{i,j}^{(PS)}(t) & \cdots & \Delta\mathbf{k}_{i,j}^{(PP)}(t) & \cdots \\ & \vdots & & \vdots & \end{bmatrix}; \quad \tilde{\mathbf{f}}(t)=\begin{bmatrix} \vdots \\ \tilde{\mathbf{f}}_i^{(S)}(t) \\ \vdots \\ \tilde{\mathbf{f}}_i^{(P)}(t) \\ \vdots \end{bmatrix}, \tag{49c,d}$$

where the time-dependent blocks $\Delta\mathbf{m}$, $\Delta\mathbf{c}$, $\Delta\mathbf{k}$ and $\tilde{\mathbf{f}}$ are defined in Appendix B. It is worth emphasizing that damping and stiffness matrices in the moving mass problem are no more symmetric. This counterintuitive result is due to the fact that the modification blocks $\Delta\mathbf{c}$ and $\Delta\mathbf{k}$ are not actual damping and stiffness contributions, but take into account the dynamic effects associated with velocity and acceleration of the moving masses (see Eqs. (B.2) and (B.3)). Importantly, the latter terms must be considered as exact contributions to the equations of motion, since the only approximation in deriving Eq. (48) for the moving mass problem is the representation of the transverse displacements for the continuous beam. Once the assumed modes are selected for the N spans, no further approximations are introduced in the solution.

5. Numerical applications

For validation purposes, the proposed SA (substructure approach) has been applied to study the vibration of two inhomogeneous multiply supported beams considered in the papers by Zheng et al. [3] (examples 2 and 3), Dugush and Eisenberger [5] (examples 1 and 2) and Martínez-Castro et al. [6] (tests 1 and 2). In the first two numerical applications reported herein, the accuracy of the proposed technique of dynamic analysis has been verified by comparing the results in terms of modal properties and moving force problem with those previously published in the literature, along with those delivered by a commercial FEM (finite element method) software (namely SAP2000, by Computers & Structures [30]). Aimed at showing versatility of the proposed SA and possible inaccuracy of the simplistic moving force model, a platoon of high-speed masses travelling along a non-prismatic continuous beam has been studied in the third numerical example.

5.1. Undamped three-span stepped beam under single moving force

In the first numerical application, the three-span continuous beam shown in Fig. 5 has been considered. The length of each span is $L_i=L/3=20$ m; the mass per unit length is constant, $\mu=1{,}000$ kg/m, but the central span has double the flexural rigidity of the side spans, $\kappa_1=\kappa_2=\kappa_3/2=1{,}960$ MN m^2. Similar to Refs. [3,5,6], the structure is assumed to be undamped ($\zeta=0$).

In a first stage, the approximate eigenproperties of the continuous beam have been computed via Eq. (41), where the matrices $\overline{\mathbf{M}}$ and $\overline{\mathbf{K}}$ have been assembled with seven assumed modes for each span (i.e. $m_i=7$ and $M=21$). The inspection of Table 2 reveals that the first five natural periods of vibration given by the proposed SA compare perfectly to the exact

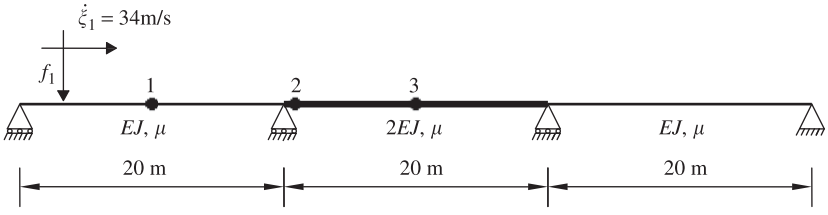

Fig. 5. Three-span stepped beam under single moving force.

Table 2
First modal periods of vibration of the stepped beam shown in Fig. 5.

Mode	Period (s)		
	Proposed SA	Ref. [5]	SAP2000
1	0.161	0.161	0.161
2	0.131	0.131	0.131
3	0.083	0.083	0.083
4	0.041	0.041	0.041
5	0.037	0.037	0.037

Comparison between proposed substructure approach (SA), exact value reported in Ref. [5] and conventional FEM analysis with SAP2000.

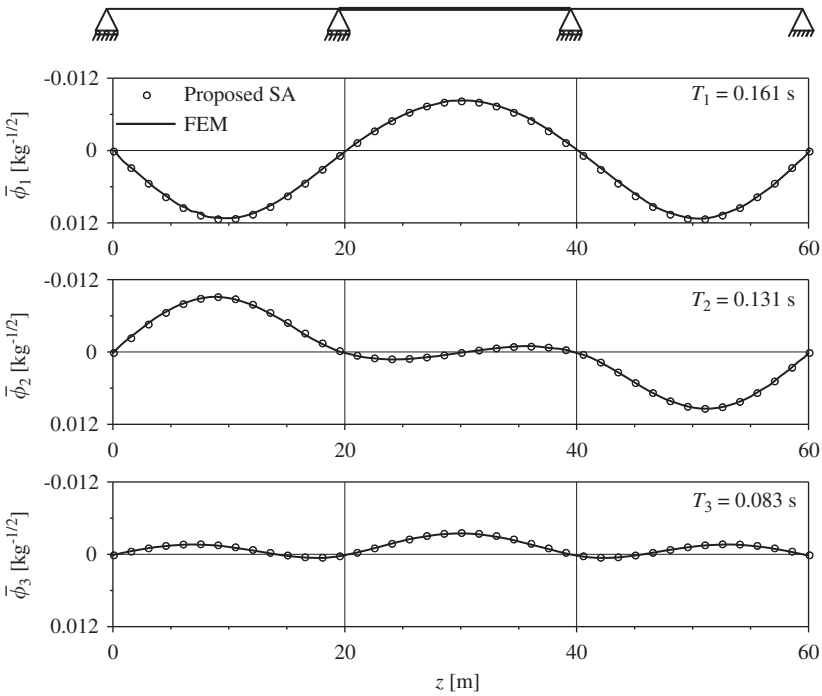

Fig. 6. First three modes of vibration of the stepped beam.

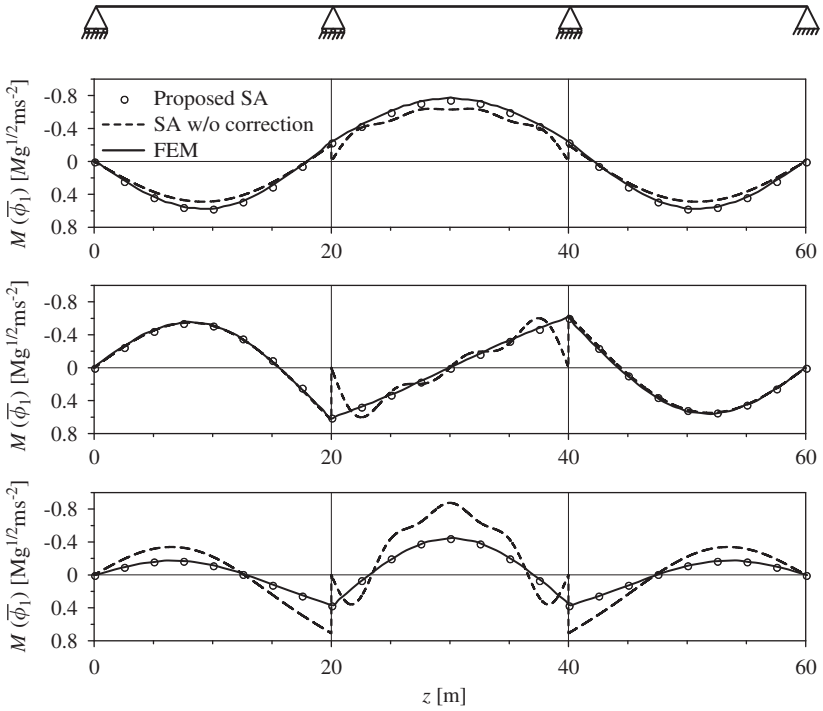

Fig. 7. First three modal bending moment diagrams of the stepped beam.

values provided in Ref. [5] and with the approximate values furnished by SAP2000 through a FEM model with 60 Euler–Bernoulli beam elements. Figs. 6 and 7 shows that proposed SA and FEM analysis are in perfect agreement in terms of modal shapes and corresponding modal bending moment (BM) diagrams, respectively. Fig. 7 highlights also the effect of the correction introduced for the central span (primary substructure) with the additional assumed modes of Eq. (16).

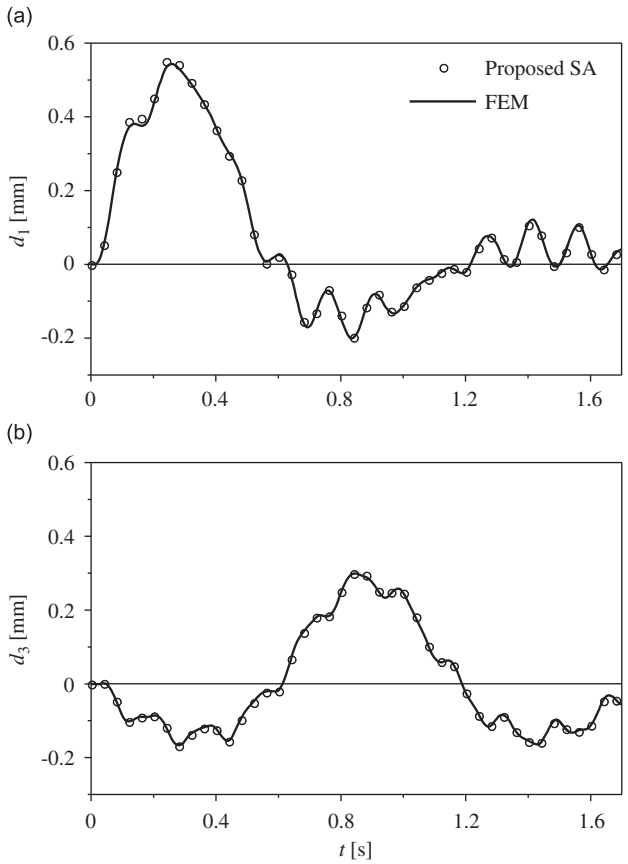

Fig. 8. Time history of the deflection experienced by the stepped beam at sections 1 (a) and 3 (b), as denoted in Fig. 5.

Indeed, a SA without this correction fails to describe accurately the BM diagram (dashed lines); on the contrary, the proposed SA with the correcting assumed modes (circles) is able to recover the FEM solution (solid lines).

In a second stage, the proposed SA has been used to compute the dynamic response due to a single force $f_1 = 9.81$ kN moving at constant speed $\dot{\xi}_1(t) = 31$ m/s($\cong 122$ km/h), and the results so obtained have been compared with those given by the FEM software. Three locations have been considered in the comparison, denoted as positions 1 (centre of the first span), 2 (first internal support) and 3 (centre of the second span) in the sketch of Fig. 5. The agreement in terms of time histories of transverse deflection at Sections 1 and 3 (Fig. 8) and BM at Sections 2 and 3 (Fig. 9) is almost perfect. Fig. 9a shows also that the accuracy in terms of BM at the position of the first internal support is completely lost without the correction for the primary span (dashed lines), in so confirming the importance to introduce the additional assumed modes of Eq. (16) for primary spans.

5.2. Undamped three-span haunched beam under single moving force

In the second application, the three-span haunched beam shown in Fig. 10 has been studied. Mass density, $\rho = 2,400$ kg/m^3, and Young's modulus, $E = 30$ GPa, do not vary along the structure. The cross section is rectangular, with constant width b=0.50 m and abscissa-dependent depth $h(z)$ varying linearly from 1.00 to 1.60 m close to the internal supports. Accordingly, the mass per unit length $\mu(z)$ varies from $\mu_{\min} = 1,200$ kg/m to $\mu_{\max} = 1,920$ kg/m, while the flexural stiffness $\kappa(z)$ varies from $\kappa_{\min} = 1,250$ MN m^2 to $\kappa_{\max} = 5,120$ MN m^2.

The length of the side (secondary) spans is L_1=L_2=18 m, whereas the length of the central (primary) span is L_3=24 m. It is worth noting that subscripts 1, 2 and 3 are here related to the numbering scheme of substructures reported in Subsection 2.1, so that the actual sequence of span's numbers in the continuous beam, from the left to the right, is 1 (secondary), 3 (primary) and 2 (secondary).

The structure vibrate under a single force f_1=100 kN travelling at constant speed $\dot{\xi}_1(t) = 17$ m/s($\cong 61$ km/h). Following Refs. [3,5,6], the damping is neglected (ζ=0).

The numerical investigations carried out for this second example confirm the effectiveness of the proposed SA. First, by using seven assumed modes for each span (i.e. m_i=7 and M=21), the first five natural periods of vibration of the continuous beam turn out to be very close to exact values reported in Ref. [5] and approximate values given by the FEM model built on

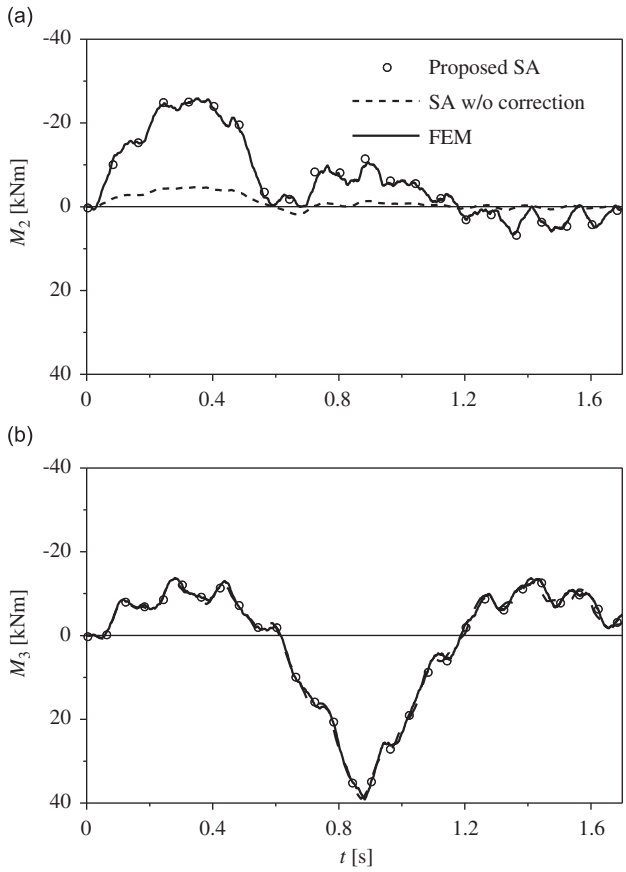

Fig. 9. Time history of the bending moment experienced by the stepped beam at sections 2 (top) and 3 (bottom), as denoted in Fig. 5.

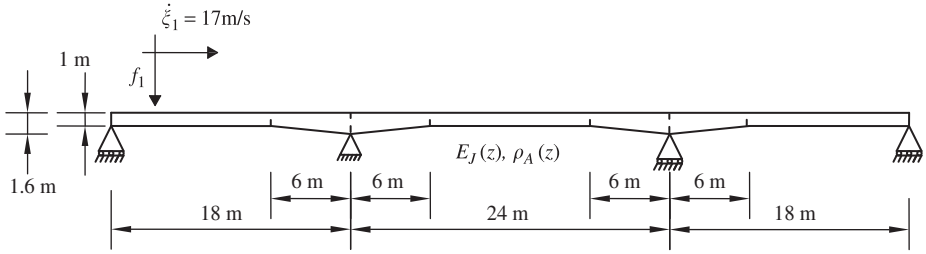

Fig. 10. Three-span haunched beam under single moving force.

Table 3
First modal periods of vibration of the haunched beam shown in Fig. 10.

Mode	Period (s)		
	Proposed SA	Ref. [5]	SAP2000
1	0.255	0.255	0.254
2	0.150	0.150	0.149
3	0.108	0.108	0.106
4	0.063	0.063	0.062
5	0.043	0.043	0.043

Comparison between proposed substructure approach (SA), exact value reported in Ref. [5] and conventional FEM analysis with SAP2000.

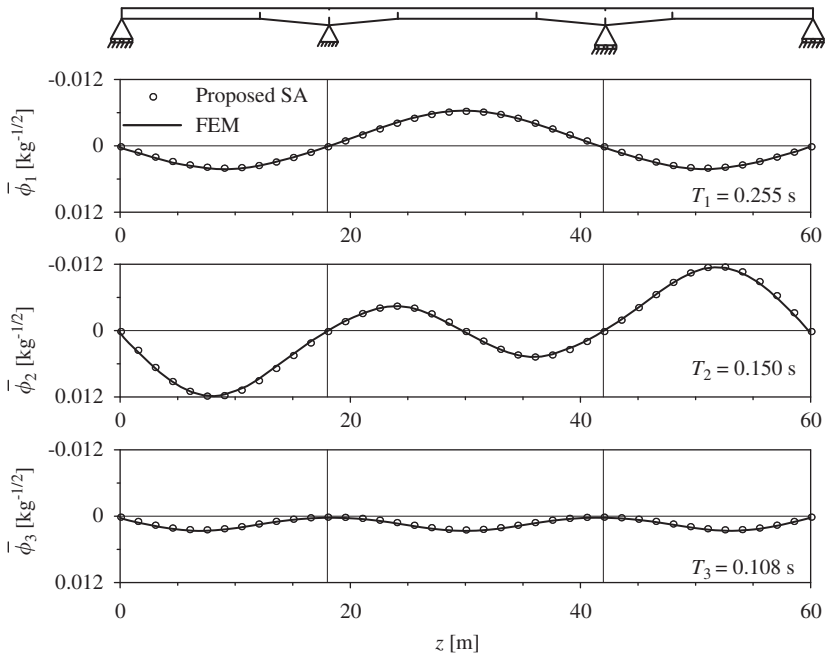

Fig. 11. First three modes of vibration of the haunched beam.

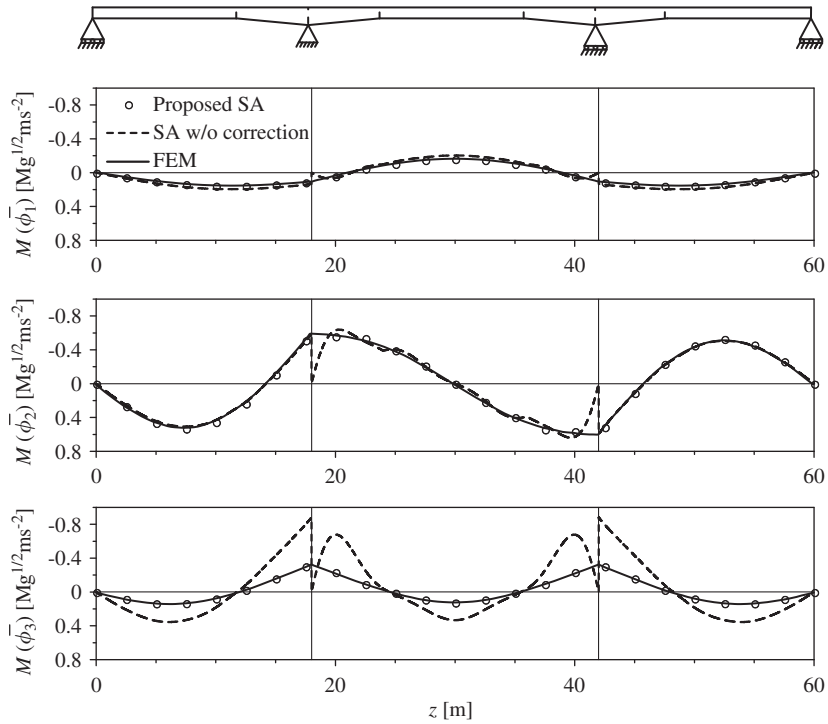

Fig. 12. First three modal bending moment diagrams of the haunched beam.

SAP2000 with 120 beam elements (see Table 3). Second, also in this case modal shapes (Fig. 11) and corresponding modal BM diagrams (Fig. 12) delivered by proposed SA (circles) and FEM model (solid lines) compare very well, and also in this case the correction introduced with the additional assumed modes of Eq. (16) is crucial in recovering the correct BM diagrams (i.e. the dashed lines plotted in Fig. 12 without this correction are unacceptable for engineering applications). This result is confirmed by Fig. 13, where the BM diagrams for two time instants of the forced vibration are shown.

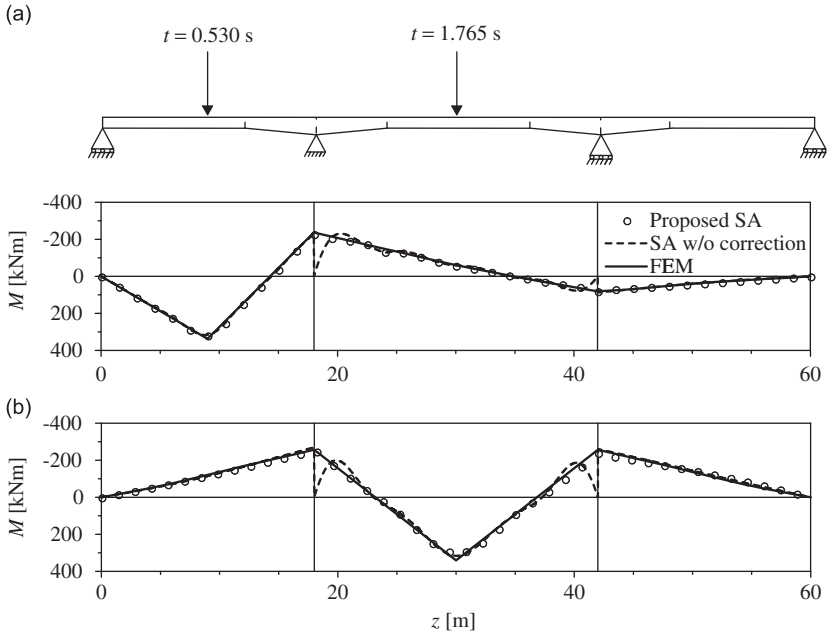

Fig. 13. Bending moment diagrams at the time instants when the moving force reaches the centre of first span (a) and second span (b).

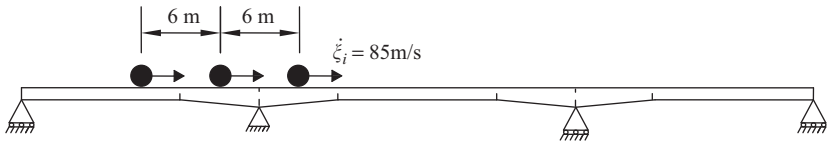

Fig. 14. Three-span haunched beam under a platoon of three moving masses.

It emerges that the SA without correction (dashed lines) fails to predict the BM at the position of the internal supports, while proposed SA (circles) and FEM model (solid lines) are always in excellent agreement.

5.3. *Damped three-span haunched beam under a platoon of moving masses*

In the third numerical application, moving force model (Section 3) and moving mass model (Section 4) have been compared, aimed at highlighting with an example the unconservative results which can be obtained when the inherent inertia of the moving loads is neglected in a realistic bridge engineering situation. To do this, the same three-span haunched beam of the previous subsection has been studied under a platoon of three identical moving masses M_i (Fig. 14), all having the same speed $\dot{\xi}_i(t) = 85\,\mathrm{m/s}(\cong 306\,\mathrm{km/h})$, which falls within the design range for actual high-speed railway bridges. The first mass enters the continuous beam at t=0, while the other two masses keep the same relative distance of 6 m. The equivalent viscous damping of the structure is assumed to be ζ=0.01 in all the modes of vibration.

Dynamic analyses have been carried out with three different intensities of the moving loads, i.e. three different platoons of moving loads have been considered with equal masses M_i of 331.2, 1,656 and 3,312 kg; the corresponding dimensionless ratios between single moving mass M_i and mass of the central span ($\int_0^{L_3} \mu_3(z_3)\,\mathrm{d}z_3$) are r_M=1.5 and 10 percent, respectively. Fig. 15 shows the results of the moving mass model in terms of dimensionless transverse displacement $d^* = 48\,d\,\kappa_{\min}/(M_1\,g\,L_3^3)$ and dimensionless BM $\mathcal{M}^* = 4\,\mathcal{M}/(M_1\,g\,L_3)$ at the middle position of the central span, which are two among the most important design parameters in practice. For comparison purposes, the results delivered by the corresponding moving force model (i.e. a group of three moving forces) are also displayed. It emerges that when the mass ratio is low (r_M=1 percent, circles), the moving force model (solid lines) is adequate; indeed, when r_M tends to zero, the dynamic modifications $\Delta\mathbf{M}(t)$, $\Delta\mathbf{C}(t)$ and $\Delta\mathbf{K}(t)$ of mass, damping and stiffness matrices (Eqs. (49)) tends to become negligible with respect to the time-independent terms $\overline{\mathbf{M}}$, $\overline{\mathbf{C}}$ and $\overline{\mathbf{K}}$ (Eqs. (39) and (41)), and the moving mass model tends to offer the same results as the moving force model. On the contrary, when the mass ratio increases to r_M=5 percent (dashed lines) and to r_M=10 percent (dotted lines), the use of mass-less moving forces leads to unconservative results, and the inaccuracy can be as large as 8.8 percent for r_M=5 percent and 18.8 percent for r_M=10 percent. It is worth noting that, according to the analytical expressions of damping and stiffness modifications provided in Appendix B (Eqs. (B.2) and

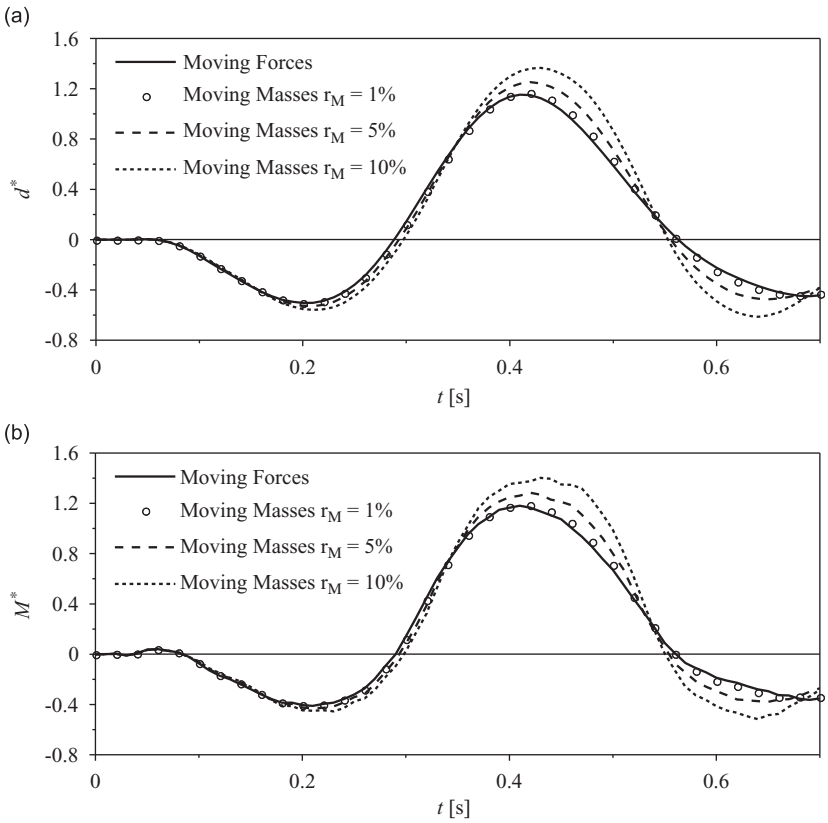

Fig. 15. Time history of dimensionless transverse deflection (a) and bending moment (b) experienced at the middle position of the central span in the haunched beam of Fig. 14.

(B.3)), this inaccuracy tends to increase with velocity and acceleration of the moving loads; as a consequence, the moving mass model seems to be much more appropriate when high-speed railway bridges are dealt with.

6. Concluding remarks

A novel substructure approach (SA) has been presented for the dynamic analysis of multiply supported slender (i.e. Euler–Bernoulli) continuous beams with varying cross section and subjected to a stream of moving loads. Based on the ideal decomposition of the whole structure into a chain of alternate primary and secondary spans, the proposed formulation builds on a special variant of the component mode synthesis (CMS) method, in which the assumed local modes for each span are taken as the exact modal shapes of the homogenized span with appropriate boundary conditions (BCs). The set of sinusoidal modes for primary pinned–pinned spans is conveniently enlarged with two cubic functions in order to represent the peak of the bending moment (BM) at the position of the intermediate supports, while for internal and side secondary spans the assumed modes are the eigenfunctions of beams with clamped–clamped and pinned–clamped BCs, respectively. The compatibility between adjacent spans is re-enforced with the help of suitable primary–secondary influence functions. (Section 2)

The Lagrange's equations of motion of the re-assembled continuous beam have been derived in the case where the moving loads are modelled either as moving forces (Section 3 and Appendix A) or moving masses (Section 4 and Appendix B), i.e. either by neglecting or including in the dynamic analysis the inherent inertia of the moving loads. In both cases the proposed formulation lends itself to be easily automated, since mass, damping and stiffness matrices are partitioned in elementary blocks, whose analytical expressions are provided in the Appendixes. It is shown that mass, damping and stiffness matrices in the moving mass model can be obtained from the analogous quantities in the moving force model (Appendix A) with some time-dependent modifications (Appendix B). Interestingly, while the mass matrix is always symmetric, damping and stiffness matrices lose this property in the moving mass model since the corresponding modifications do not represent actual dissipations and rigidities, but the inertial effects associated with velocity and acceleration of the moving masses.

Two numerical applications with the moving force model demonstrate that the results obtained with the proposed SA are in excellent agreement with those of previously published investigations, along with those delivered by a standard FEM

(finite element method) software. A third numerical application with the moving mass model shows the versatility of the proposed formulation, and is also used to quantify the possible inaccuracy of the moving force model.

Acknowledgements

This study has been partially funded by the Italian Ministry of Education, University and Scientific Research (MIUR), under 2007–2009 PRIN Grant on "Dynamic behaviour of structures in linear and nonlinear range". Most of the numerical results have been obtained when AP and VDS were Lecturer in Civil Engineering and visiting PhD student, respectively, within the School of Engineering, Design and Technology at the University of Bradford, whose support in kind is gratefully acknowledged.

Appendix A. Mass, stiffness and loading terms in the moving force problem

The mass sub-matrices in Eq. (39) can be evaluated through the following integrals:

$$\overline{\mathbf{m}}_{i,i}^{(\mathrm{SS})} = \rho \int_0^{L_i} A_i(z_i)\boldsymbol{\phi}_i(z_i)\cdot\boldsymbol{\phi}_i^T(z_i)\mathrm{d}z_i; \tag{A.1a}$$

$$\overline{\mathbf{m}}_{i,j}^{(\mathrm{SP})} = \rho \int_0^{L_i} A_i(z_i)\boldsymbol{\phi}_i(z_i)\cdot\boldsymbol{\psi}_{i,j}^T(z_i)\mathrm{d}z_i = \left[\mathbf{m}_{j,i}^{(\mathrm{PS})}\right]^{\mathrm{T}}; \tag{A.1b}$$

$$\overline{\mathbf{m}}_{i,j}^{(\mathrm{PP})} = \left[\rho \int_0^{L_i} A_i(z_i)\boldsymbol{\phi}_i(z_i)\cdot\boldsymbol{\phi}_j^T(z_i)\mathrm{d}z_i\right]\delta_{i,j} + \rho\sum_{r=1}^{n_S}\left[\int_0^{L_r} A_r(z_r)\boldsymbol{\psi}_{r,i}(z_r)\cdot\boldsymbol{\psi}_{r,j}^T(z_r)\mathrm{d}z_r\right], \tag{A.1c}$$

where the superscripts (P) and (S) stand for primary and secondary spans, respectively.

The stiffness sub-matrices are given by

$$\overline{\mathbf{k}}_{i,i}^{(\mathrm{SS})} = E\int_0^{L_i} J_i(z_i)\boldsymbol{\phi}_i''(z_i)\cdot\{\boldsymbol{\phi}_i''(z_i)\}^{\mathrm{T}}\mathrm{d}z_i; \tag{A.2a}$$

$$\overline{\mathbf{k}}_{i,j}^{(\mathrm{PP})} = \left[E\int_0^{L_i} J_i(z_i)\boldsymbol{\phi}_i''(z_i)\cdot\{\boldsymbol{\phi}_j''(z_i)\}^{\mathrm{T}}\mathrm{d}z_i\right]\delta_{i,j} + E\sum_{r=1}^{n_S}\left[\int_0^{L_r} J_r(z_r)\boldsymbol{\psi}_{r,i}''(z_r)\cdot\{\boldsymbol{\psi}_{r,j}''(z_r)\}^{\mathrm{T}}\mathrm{d}z_r\right]. \tag{A.2b}$$

Finally, the loading terms are so defined:

$$\overline{\mathbf{f}}_i^{(\mathrm{S})}(t) = g\rho\int_0^{L_i} A_i(z_i)\boldsymbol{\phi}_i(z_i)\,\mathrm{d}z_i + \sum_{k=1}^{n_F} f_k\chi_i(\xi_k(t)-\overline{z}_i)\boldsymbol{\phi}_i(\xi_k(t)-\overline{z}_i); \tag{A.3a}$$

$$\begin{aligned}\overline{\mathbf{f}}_i^{(\mathrm{P})}(t) = {} & g\rho\left\{\int_0^{L_i} A_i(z_i)\boldsymbol{\phi}_i(z_i)\mathrm{d}z_i + \sum_{r=1}^{n_S}\int_0^{L_r} A_r(z_i)\boldsymbol{\psi}_{r,i}(z_r)\mathrm{d}z_r\right\} + \sum_{k=1}^{n_F} f_k\chi_i(\xi_k(t)-\overline{z}_i)\boldsymbol{\phi}_i(\xi_k(t)-\overline{z}_i)\\ & + \sum_{r=1}^{n_S}\sum_{k=1}^{n_F} f_k\chi_r(\xi_k(t)-\overline{z}_r)\boldsymbol{\psi}_{r,i}(\xi_k(t)-\overline{z}_r).\end{aligned} \tag{A.3b}$$

Appendix B. Mass, stiffness and loading terms in the moving mass problem

The mass sub-matrices in Eqs. (49) are given by

$$\Delta\mathbf{m}_{i,i}^{(\mathrm{SS})}(t) = \sum_{k=1}^{n_M} M_k\boldsymbol{\phi}_i(\xi_k(t)-\overline{z}_i)\cdot\boldsymbol{\phi}_i^T(\xi_k(t)-\overline{z}_i)\chi_i(\xi_k(t)-\overline{z}_i); \tag{B.1a}$$

$$\Delta\mathbf{m}_{i,j}^{(\mathrm{SP})}(t) = \sum_{k=1}^{n_M} M_k\boldsymbol{\phi}_i(\xi_k(t)-\overline{z}_i)\cdot\boldsymbol{\psi}_{i,j}^T(\xi_k(t)-\overline{z}_i)\chi_i(\xi_k(t)-\overline{z}_i) = \left[\Delta\mathbf{m}_{i,j}^{(\mathrm{PS})}(t)\right]^{\mathrm{T}}; \tag{B.1b}$$

$$\begin{aligned}\Delta\mathbf{m}_{i,j}^{(\mathrm{PP})}(t) = {} & \left[\sum_{k=1}^{n_M} M_k\boldsymbol{\phi}_i(\xi_k(t)-\overline{z}_i)\cdot\boldsymbol{\phi}_j^T(\xi_k(t)-\overline{z}_i)\chi_i(\xi_k(t)-\overline{z}_i)\right]\delta_{i,j}\\ & + \sum_{k=1}^{n_M}\sum_{r=1}^{n_S} M_k\boldsymbol{\psi}_{r,i}(\xi_k(t)-\overline{z}_r)\cdot\boldsymbol{\psi}_{r,j}^T(\xi_k(t)-\overline{z}_r)\chi_r(\xi_k(t)-\overline{z}_r).\end{aligned} \tag{B.1c}$$

The damping-like sub-matrices can be evaluated through the following summations:

$$\Delta\mathbf{c}_{i,i}^{(\mathrm{SS})}(t)=2\sum_{k=1}^{n_M}M_k\dot{\xi}_k(t)\boldsymbol{\phi}_i(\xi_k(t)-\overline{z}_i)\cdot(\boldsymbol{\phi}_i'(\xi_k(t)-\overline{z}_i))^{\mathrm{T}}\chi_i(\xi_k(t)-\overline{z}_i); \tag{B.2a}$$

$$\Delta\mathbf{c}_{i,j}^{(\mathrm{SP})}(t)=2\sum_{k=1}^{n_M}M_k\dot{\xi}_k(t)\boldsymbol{\phi}_i(\xi_k(t)-\overline{z}_i)\cdot\{\boldsymbol{\psi}_{i,j}'(\xi_k(t)-\overline{z}_i)\}^{\mathrm{T}}\chi_i(\xi_k(t)-\overline{z}_i); \tag{B.2b}$$

$$\Delta\mathbf{c}_{i,j}^{(\mathrm{PS})}(t)=2\sum_{k=1}^{n_M}M_k\dot{\xi}_k(t)\boldsymbol{\psi}_{j,i}(\xi_k(t)-\overline{z}_j)\cdot\{\boldsymbol{\phi}_j'(\xi_k(t)-\overline{z}_j)\}^{\mathrm{T}}\chi_j(\xi_k(t)-\overline{z}_j); \tag{B.2c}$$

$$\begin{aligned}\Delta\mathbf{c}_{i,j}^{(\mathrm{PP})}(t)=&\left[2\sum_{k=1}^{n_M}M_k\dot{\xi}_k(t)\boldsymbol{\phi}_i(\xi_k(t)-\overline{z}_i)\cdot\{\boldsymbol{\phi}_i'(\xi_k(t)-\overline{z}_i)\}^{\mathrm{T}}\chi_i(\xi_k(t)-\overline{z}_i)\right]\delta_{ij}\\&+2\sum_{k=1}^{n_M}\sum_{r=1}^{n_S}M_k\dot{\xi}_k(t)\boldsymbol{\psi}_{r,i}(\xi_k(t)-\overline{z}_r)\cdot\{\boldsymbol{\psi}_{r,j}'(\xi_k(t)-\overline{z}_r)\}^{\mathrm{T}}\chi_r(\xi_k(t)-\overline{z}_r).\end{aligned} \tag{B.2d}$$

The stiffness-like sub-matrices take the form:

$$\Delta\mathbf{k}_{i,i}^{(\mathrm{SS})}(t)=\sum_{k=1}^{n_M}M_k\left[\ddot{\xi}_k(t)\boldsymbol{\phi}_i'(\xi_k(t)-\overline{z}_i)\cdot\{\boldsymbol{\phi}_i'(\xi_k(t)-\overline{z}_i)\}^{\mathrm{T}}+\dot{\xi}_k^2(t)\boldsymbol{\phi}_i(\xi_k(t)-\overline{z}_i)\cdot\{\boldsymbol{\phi}_i''(\xi_k(t)-\overline{z}_i)\}^{\mathrm{T}}\right]\chi_i(\xi_k(t)-\overline{z}_i); \tag{B.3a}$$

$$\Delta\mathbf{k}_{i,j}^{(\mathrm{SP})}(t)=\sum_{k=1}^{n_M}M_k\left[\ddot{\xi}_k(t)\boldsymbol{\phi}_i(\xi_k(t)-\overline{z}_i)\cdot\{\boldsymbol{\psi}_{i,j}'(\xi_k(t)-\overline{z}_i)\}^{\mathrm{T}}+\dot{\xi}_k^2(t)\boldsymbol{\phi}_i(\xi_k(t)-\overline{z}_i)\cdot\{\boldsymbol{\psi}_{i,j}''(\xi_k(t)-\overline{z}_i)\}^{\mathrm{T}}\right]\chi_i(\xi_k(t)-\overline{z}_i); \tag{B.3b}$$

$$\Delta\mathbf{k}_{i,j}^{(\mathrm{PS})}(t)=\sum_{k=1}^{n_M}M_k\left[\ddot{\xi}_k(t)\boldsymbol{\psi}_{j,i}(\xi_k(t)-\overline{z}_j)\cdot\{\boldsymbol{\phi}_j'(\xi_k(t)-\overline{z}_j)\}^{\mathrm{T}}+\dot{\xi}_k^2(t)\boldsymbol{\psi}_{j,i}(\xi_k(t)-\overline{z}_j)\cdot\{\boldsymbol{\phi}_j''(\xi_k(t)-\overline{z}_j)\}^{\mathrm{T}}\right]\chi_j(\xi_k(t)-\overline{z}_j); \tag{B.3c}$$

$$\begin{aligned}\Delta\mathbf{k}_{i,j}^{(\mathrm{PP})}(t)=&\sum_{k=1}^{n_M}M_k\Big[\ddot{\xi}_k(t)\boldsymbol{\phi}_i(\xi_k(t)-\overline{z}_i)\cdot\{\boldsymbol{\phi}_j'(\xi_k(t)-\overline{z}_i)\}^{\mathrm{T}}+\dot{\xi}_k^2(t)\boldsymbol{\phi}_i(\xi_k(t)-\overline{z}_i)\cdot\{\boldsymbol{\phi}_j''(\xi_k(t)-\overline{z}_i)\}^{\mathrm{T}}]\chi_i(\xi_k(t)-\overline{z}_i)\delta_{i,j}\\&+\sum_{k=1}^{n_M}\sum_{r=1}^{n_S}M_k[\ddot{\xi}_k(t)\boldsymbol{\psi}_{r,i}(\xi_k(t)-\overline{z}_r)\cdot\{\boldsymbol{\psi}_{r,j}'(\xi_k(t)-\overline{z}_r)\}^{\mathrm{T}}+\dot{\xi}_k^2(t)\boldsymbol{\psi}_{r,i}(\xi_k(t)-\overline{z}_r)\cdot\{\boldsymbol{\psi}_{r,j}''(\xi_k(t)-\overline{z}_r)\}^{\mathrm{T}}\Big]\chi_r(\xi_k(t)-\overline{z}_r).\end{aligned} \tag{B.3d}$$

Finally, the loading terms are so defined

$$\tilde{\mathbf{f}}_i^{(\mathrm{S})}(t)=g\left\{\rho\int_0^{L_i}A_i(z_i)\boldsymbol{\phi}_i(z_i)\mathrm{d}z_i+\sum_{k=1}^{n_M}M_k\boldsymbol{\phi}_i(\xi_k(t)-\overline{z}_i)\chi_i(\xi_k(t)-\overline{z}_i)\right\}; \tag{B.4a}$$

$$\begin{aligned}\tilde{\mathbf{f}}_i^{(\mathrm{P})}(t)=&g\rho\left\{\int_0^{L_i}A_i(z_i)\boldsymbol{\phi}_i(z_i)\mathrm{d}z_i+\sum_{r=1}^{n_S}\int_0^{L_r}A_r(z_i)\boldsymbol{\psi}_{r,i}(z_r)\mathrm{d}z_r\right\}+\sum_{k=1}^{n_M}f_k\boldsymbol{\phi}_i(\xi_k(t)-\overline{z}_i)\chi_i(\xi_k(t)-\overline{z}_i)\\&+\sum_{k=1}^{n_M}\sum_{r=1}^{n_S}f_k\boldsymbol{\psi}_{r,i}(\xi_k(t)-\overline{z}_r)\chi_r(\xi_k(t)-\overline{z}_r),\end{aligned} \tag{B.4b}$$

where $f_k=M_kg$.

References

[1] H.P. Lee, Dynamic response of a beam with intermediate point constraints subjected to a moving load, *Journal of Sound and Vibration* 171 (1994) 361–368.

[2] H.P. Lee, Dynamic response of a beam on multiple supports with a moving mass, *Structural Engineering and Mechanics* 4 (1996) 303–312.

[3] D.Y. Zheng, Y.K. Cheung, F.T.K. Au, Y.S. Cheng, Vibration of multi-span non-uniform beams under moving loads by using modified beam vibration functions, *Journal of Sound and Vibration* 212 (1998) 455–467.

[4] M. Ichikawa, Y. Miyakawa, A. Matsuda, Vibration analysis of the continuous beam subjected to a moving mass, *Journal of Sound and Vibration* 230 (2000) 493–506.

[5] Y.A. Dugush, M. Eisenberger, Vibrations of non-uniform continuous beams under moving loads, *Journal of Sound and Vibration* 254 (2002) 911–926.

[6] A.E. Martínez-Castro, P. Museros, A. Castello-Linares, Semi-analytic solution in the time domain for non-uniform multi-span Bernoulli-Euler beams traversed by moving loads, *Journal of Sound and Vibration* 294 (2006) 278–297.

[7] D. Stăncioiu, H. Ouyang, J.E. Mottershead, Vibration of a continuous beam with multiple elastic supports excited by a moving two-axle system with separation, *Meccanica* 44 (2009) 293–303.

[8] H. Xu, W.L. Li, Dynamic behavior of multi-span bridges under moving loads with focusing on the effect of the coupling conditions between spans, *Journal of Sound and Vibration* 312 (2008) 736–753.
[9] X.Q. Zhu, S.S. Law, Moving load identification on multi-span continuous bridges with elastic bearings, *Mechanical Systems and Signal Processing* 20 (2006) 1759–1782.
[10] E. Paraskevopoulos, C. Panagiotopoulos, D. Talaslidis, Rational derivation of conserving time integration schemes: the moving-mass case, in: M. Papadrakakis, D.C. Charmpis, Y. Tsompanakis, N.D. Lagaros (Eds.), *Computational Structural Dynamics and Earthquake Engineering*, CRC Press, Boca Raton, 2006, pp. 149–164.
[11] W. Lacarbonara, V. Colone, Dynamic response of arch bridges traversed by high-speed trains, *Journal of Sound and Vibration* 304 (2007) 72–90.
[12] N. Zhang, H. Xia, W. Guo, Vehicle–bridge interaction analysis under high-speed trains, *Journal of Sound and Vibration* 309 (2008) 407–425.
[13] K. Liu, E. Reynders, G. De Roeck, G. Lombaert, Experimental and numerical analysis of a composite bridge for high-speed trains, *Journal of Sound and Vibration* 320 (2009) 201–220.
[14] W.C. Hurty, Vibrations of structural systems by component mode synthesis, *Journal of Engineering Mechanics Division* 86 (1960) 51–69.
[15] R.R. Craig Jr., Substructure methods in vibration, *Journal of Mechanical Design, Transactions of the ASME* 117B (1995) 207–213.
[16] B. Biondi, G. Muscolino, Component-mode synthesis method variants in the dynamics of coupled structures, *Meccanica* 35 (2000) 17–38.
[17] G. Muscolino, Dynamic analysis of structural systems using component mode synthesis, in: B.H.V. Topping, Z. Bittnar (Eds.), *Computational Structures Technology*, Saxe-Coburg Publications, Stirling, 2002, pp. 255–282.
[18] B. Biondi, G. Muscolino, Component-mode synthesis method for coupled continuous and FE discretized substructures, *Engineering Structures* 25 (2003) 419–433.
[19] B. Biondi, G. Muscolino, A. Sofi, A substructure approach for the dynamic analysis of train-track-bridge system, *Computers and Structures* 83 (2005) 2271–2281.
[20] Y. Tang, Numerical evaluation of uniform beam modes, *Journal of Engineering Mechanics* 129 (2003) 1475–1477.
[21] G. Muscolino, A. Palmeri, A. Sofi, Absolute versus relative formulations of the moving oscillator problem, *International Journal of Solids and Structures* 46 (2009) 1085–1094.
[22] L. Meirovitch, *Methods of Analytical Dynamics*, Dover, New York, 1970 republished 2003.
[23] R.W. Clough, J. Penzien, *Dynamics of Structures*, second ed, McGraw-Hill, New York, 1993.
[24] B. Balachandran, E.B. Magrab, *Vibrations*, second ed, Cengage, Toronto, 2009.
[25] M.N. Newmark, A method of computation for structural dynamics, *Journal of the Engineering Mechanics Division* 85 (1959) 67–94.
[26] B. Biondi, G. Muscolino, G. Sidoti, Methods for calculating bending moment and shear force in the moving mass problem, *Journal of Vibration and Acoustics, Transactions of the ASME* 126 (2004) 542–552.
[27] S. Sadiku, H.H.E. Leipholz, On the dynamics of elastic systems with moving concentrated masses, *Ingenieur-Archiv* 57 (1987) 223–242.
[28] G. Michaltsos, D. Sophianopoulos, A.N. Kounadis, The effect of a moving mass and other parameters on the dynamic response of a simply supported beam, *Journal of Sound and Vibration* 191 (1996) 357–362.
[29] C. Bilello, L.A. Bergman, D. Kuchma, Experimental investigation of a small-scale bridge model under a moving mass, *Journal of Structural Engineering* 130 (2004) 799–804.
[30] SAP2000 (computer program), release 11.0, Computers and Structures, Berkeley, 2007.